22

Superhydrophobic and Superoleophobic Nanostructured Cellulose and Cellulose Composites

Robin H. A. Ras[1], *Xuelin Tian*[1,2], *and Ilker S. Bayer*[3]

[1] *Department of Applied Physics, Aalto University School of Science, Puumiehenkuja 2, 02150 Espoo, Finland*
[2] *Sun Yat-sen University, School of Materials Science and Engineering, Guangzhou 510275, China*
[3] *Smart Materials, Istituto Italiano di Tecnologia, Via Morego 30, 16163 Genova, Italy*

Abstract

Superhydrophobic and superoleophobic surfaces are extremely liquid repellent and attract global interest from researchers, industry, and laymen. Arguably the main appeal is their dirt-repellent features, though superhydrophobic surfaces are also antifogging and anti-icing and remain dry underwater. Cellulose is an excellent building material for superhydrophobic surfaces, as is demonstrated by plants, such as lotus and cabbage leaves. Also for technological applications, cellulose is attractive because it is a cheap, green, sustainable, and versatile nanomaterial that allows easy modifications. Here we review the recent advances in nonwetting cellulose materials, and in particular water-repellent and oil-repellent nanocelluloses, such as cellulose nanofibers and nanowhiskers.

Keywords *superhydrophobic; superoleophobic; nonwetting; hydrophobic; nanocellulose*

List of Abbreviations

θ_Y	Young's contact angle
θ	apparent contact angle
θ_A	advancing contact angle
θ_R	receding contact angle
γ_{sg}	solid–gas interfacial tension
γ_{sl}	solid–liquid interfacial tension
γ_{lg}	liquid–gas interfacial tension
r	surface roughness factor
f	solid–liquid contact fraction
F_p	hysteresis force
w	droplet–surface contact radius

Handbook of Nanocellulose and Cellulose Nanocomposites, First Edition.
Edited by Hanieh Kargarzadeh, Ishak Ahmad, Sabu Thomas, and Alain Dufresne.

AFM	atomic force microscope
AKD	alkyl ketene dimer
ALD	atomic layer deposition
CA	cellulose acetate
CLE	cellulose lauroyl ester
CNFs	cellulose nanofibrils
CTA	cellulose triacetate
DMA	dynamic mechanical analysis
EtOH	ethanol
FTIR	Fourier transform infrared spectroscopy
MC	methylene chloride
MFC	microfibrillated cellulose
NFC	nanofibrillated cellulose
PCC	precipitated calcium carbonate
SEM	scanning electron microscopy
SBR	synthetic rubber
TEMPO	2,2,6,6-tetramethylpiperidine-1-oxyl
TOCN	2,2,6,6-tetramethylpiperidine-1-oxyl-oxidized cellulose nanomaterials
TW	cellulose nanowhiskers isolated from tunicates
XPS	X-ray photoelectron spectroscopy
WCA	water contact angle
ZnO	zinc oxide

22.1 Introduction

Superhydrophobic and superoleophobic surfaces are extremely liquid repellent and attract global interest from researchers, industry, and laymen [1–11]. Arguably the main appeal is their dirt-repellent features, though superhydrophobic surfaces are also antifogging and anti-icing and remain dry underwater. Cellulose is an excellent building material for superhydrophobic surfaces, as is demonstrated by plants, such as lotus and cabbage leaves [12, 13]. Also for technological applications, cellulose is attractive because it is a cheap, green, sustainable, and versatile nanomaterial that allows easy modifications [14–23]. Here we review the recent advances in nonwetting cellulose materials, and in particular water-repellent and oil-repellent nanocellulose, such as cellulose nanofibers and nanowhiskers.

From wetting point of view, nanostructured cellulose and cellulose composites offer a wide range of application possibilities. These can be summarized as green and biodegradable textured surfaces for control of wetting, templates with tunable roughness for hydrophobicity, bio-based filters for oil–water separation, and green materials for biofouling and printing [24]. There are numerous ways of fabricating nanostructured cellulose materials and cellulose composites. Some methods are based on complete dissolution of cellulose, followed by controlled regeneration; other methods break the micron-sized cellulose fibers down in a controlled manner to nanoscale building blocks, such as cellulose nanofibers

and cellulose nanocrystals, keeping the native cellulose I crystal structure intact [15, 25, 26]. The resulting nanostructures include aerogels [27] and foams [28], nanofibers by electrospinning, and etching of cellulosic microfibers to form nanostructures and templates [29, 30].

The first part of the chapter deals with the basics of wetting and outlines a general procedure for wetting analysis by contact angle measurement. Often only static contact angles are reported, whereas advancing and receding contact angles are needed for a rigorous evaluation of wetting, preferably combined with measurement of the sliding angle. For water-repellent surfaces, the difference between advancing and receding contact angles, that is, contact angle hysteresis, is a very relevant property, as it is directly related to the force that keeps a droplet pinned.

In the second part of the chapter, we present fabrication, performance, and applications of superhydrophobic materials comprising nanostructured cellulose, cellulose derivatives, and composites. Due to extreme environmental importance of cellulose and its abundance, renewability, and low cost, nanostructured cellulose can eventually be the material of choice for the fabrication of various types of liquid-repellent materials [30–32]. As such it can find widespread applications in filtration, water purification, biofouling, and biomedical areas, such as tissue engineering and drug delivery.

22.2 Key Principles of Wetting Characterization

22.2.1 Young's Equation and Superhydrophobicity/Superoleophobicity

Wettability is a fundamental property of functional surface materials. The contact angle of a liquid on an ideal, flat, and homogeneous solid surface is determined by interfacial tensions of the three-phase (solid–liquid–gas) system (Figure 22.1). It characterizes the competitive affinity interaction with the solid surface between the liquid and the gas and is quantified by the well-known Young equation [33]:

$$\cos\theta_Y = \frac{\gamma_{sg} - \gamma_{sl}}{\gamma_{lg}} \tag{22.1}$$

where θ_Y is Young's contact angle on the solid surface and γ_{sg}, γ_{sl}, and γ_{lg} are the interfacial tensions between solid–gas, solid–liquid, and liquid–gas, respectively. It is important to note that Eq. (22.1) defines the state in which the system has the minimum total interfacial free energy.

When a surface displays a contact angle less than 90° with water or oil, it is considered as hydrophilic or oleophilic, whereas when the contact angle is

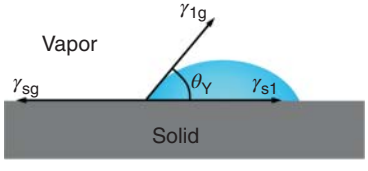

Figure 22.1 Wetting on a solid surface.

larger than 90°, it is considered as hydrophobic or oleophobic. The extremely interesting surfaces that have received tremendous research interest in recent years are superhydrophobic/superoleophobic surfaces, owing to their potential applications in various technological fields, such as in self-cleaning, anti-icing, antismudge, drag reduction, and nonloss transportation [34, 35].

Generally, a surface is regarded as superhydrophobic/superoleophobic when it exhibits a water/oil contact angle larger than 150°, and meanwhile a water/oil droplet can slide away from the surface easily. Such surfaces can be prepared by combination of low surface energy coating and appropriate surface roughness. Two basic models were developed to understand wetting phenomena on rough surfaces. The first model was proposed by Wenzel [36], which deals with the situation in which the liquid penetrates into the surface roughness (Figure 22.2a). The contact angle θ of a Wenzel state droplet is given by

$$\cos\theta = r\cos\theta_{\mathrm{Y}} \tag{22.2}$$

where r is the surface roughness factor, that is, the ratio of the actual surface area to its geometric projected area. As r is always larger than 1, it is easy to understand that roughness can amplify surface hydrophobicity for a material with $\theta_{\mathrm{Y}} > 90°$ and even endow a surface with $\theta > 150°$. However, a Wenzel droplet generally remains in highly sticky state on a surface and does not slide away since the liquid keeps intimate contact with underlying surface texture.

Another model, that is, the Cassie–Baxter model [37], deals with the situation in which the liquid is suspended by a composite solid–gas interface (Figure 22.2b), and the contact angle is given by [38]

$$\cos\theta = r_{\mathrm{f}} f\cos\theta_{\mathrm{Y}} - (1-f) \tag{22.3}$$

where f is the solid–liquid contact fraction, r_{f} is the roughness factor of the wetted solid part (which is 1 for commonly seen microfabricated straight posts), and $1-f$ represents the air–liquid contact fraction. Droplets in Cassie–Baxter state contact only a fraction of the underlying solid surface and thus can be highly mobile and readily slide away from the surface.

Both Wenzel and Cassie–Baxter equations can be derived from Young's equation, and the contact angle obtained from Eqs. (22.2) and (22.3) represents the energetically most favorable state for a Wenzel-type droplet or Cassie–Baxter-type droplet, respectively. The most stable state is the lower free

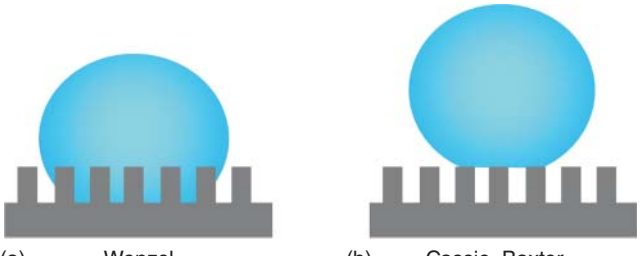

Figure 22.2 Wetting on rough surfaces: (a) Wenzel and (b) Cassie–Baxter wetting states.

energy state of these two states, which can be identified according to a critical contact angle [39]:

$$\cos\theta_t = \frac{f-1}{r-r_f f} \tag{22.4}$$

If $\theta_Y < \theta_t$, the Wenzel state given by Eq. (22.2) is the thermodynamically most stable state, whereas when $\theta_Y > \theta_t$, the Cassie–Baxter state given by Eq. (22.3) is the most stable state.

22.2.2 Contact Angle Hysteresis

In experimental measurement of contact angles on real surfaces, a number of different contact angles rather than a specific contact angle may be obtained depending on measuring procedure. These practical contact angles are located within a range confined to two characteristic contact angles, namely, the advancing and receding contact angles. The advancing contact angle θ_A can be measured by gradually increasing the volume of a sessile droplet until the solid–liquid–gas contact line begins to expand (Figure 22.3a), at which time a maximum contact angle, that is, θ_A, is reached. The receding contact angle θ_R is measured by gradually decreasing the volume of a sessile droplet until the contact line begins to shrink, at which time θ_R is obtained (Figure 22.3b). The difference between θ_A and θ_R (or between their cosines) is called contact angle hysteresis.

Contact angle hysteresis is generally considered to be caused by either chemical heterogeneity or geometrical roughness on surfaces. On a surface with geometrical heterogeneity, the apparent contact angle depends on both Young's contact angle and surface morphology. On a nonflat surface schematically shown

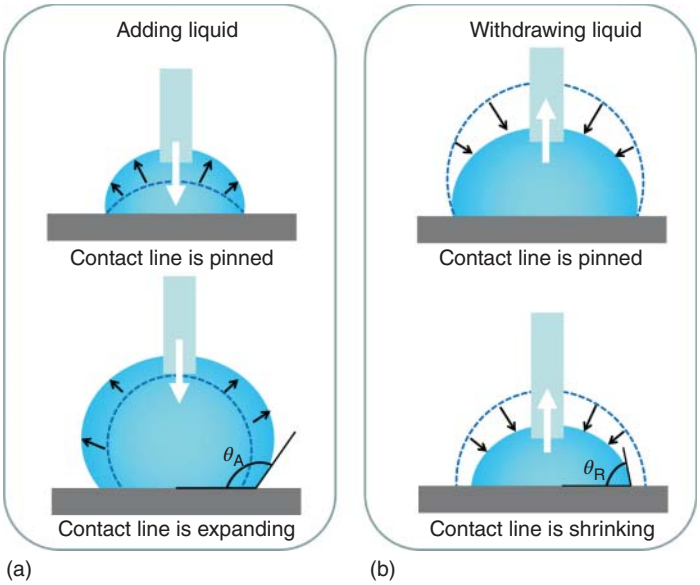

Figure 22.3 Measurement of (a) advancing and (b) receding contact angles. The advancing or receding contact angle is obtained only after the contact line starts moving.

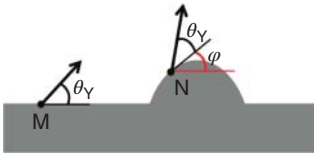

Figure 22.4 Effect of surface roughness on apparent contact angle. The apparent contact angle varies with location to keep Young's contact angle conform to local surface morphology.

in Figure 22.4, the apparent contact angle at location N is the sum of θ_Y and φ, where φ is the local slope. Thus roughness will lead to varying apparent contact angles along the surface due to the morphology undulation. Chemical heterogeneity leads to varying Young's contact angles along a surface, which certainly changes the apparent contact angle. Therefore, both chemical and geometrical heterogeneity can result in continuously changing apparent contact angles along a surface. When a droplet is deposited on a surface, the contact angle it adopts must be equal to the local apparent contact angle where the contact line locates. At the same time, the droplet has to satisfy a geometrical criterion, that is, its contact area with the solid determines a geometrical contact angle due to the droplet volume constraint. The system acquires a local minimum in total interfacial free energy only when the geometrical contact angle is equal to the local apparent contact angle [40, 41]. For a given droplet–surface system, a number of local minimums could be obtained (Figure 22.5), including a global minimum and many metastable states. The advancing contact angle θ_A can then be considered as the highest contact angle that a local minimum allows, and the receding contact angle θ_R is the lowest contact angle that a local minimum allows. Note that the theoretically highest or lowest contact angles, which represent two metastable states of highest interfacial free energy, may be not experimentally accessible because environmental disturbance could drive the system to overcome certain energy barrier to reach metastable states of lower free energy. Therefore, experimentally measured θ_A may be lower than theoretical θ_A, whereas the experimental θ_R may be larger than the theoretical θ_R. For reliable measurement of θ_R, it is important that initial drop size is sufficiently large [42].

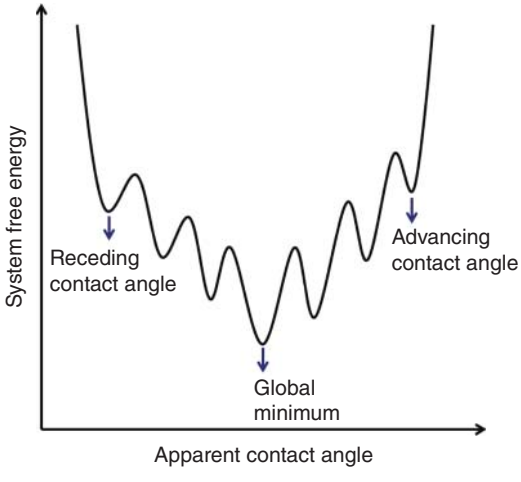

Figure 22.5 Schematic illustration of the relationship between interfacial free energy and apparent contact angle for a droplet–surface–gas system.

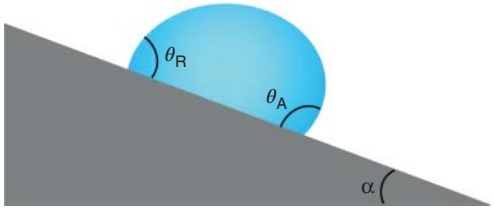

Figure 22.6 Pinning behavior of a droplet on a surface. The largest pinning force is obtained when the advancing side and the receding side of the droplet reach a contact angle of θ_A and θ_R, respectively.

The advancing contact angle and the receding contact angle are important in determining the mobility of a droplet on a surface. Macdougall and Ockrent [43] found that the lateral pinning force that resists the movement of a droplet on an inclined surface is proportional to $\cos\theta_R - \cos\theta_A$ (Figure 22.6). Such relationship was confirmed by different investigators [44, 45], and the pinning force can be described as

$$F_p = kw\gamma_{lg}(\cos\theta_R - \cos\theta_A) \tag{22.5}$$

where k is a constant and w is the radius of droplet base. The constant k can be reasonably regarded as close to 2 in quantitative calculation. In case a pinned droplet is severely deformed on a surface, the contact base will not be an axisymmetric circle, and w in Eq. (22.5) should be replaced by the half width of the base perpendicular to the droplet moving direction. The aforementioned relationship indicates both large contact angle (which reduces the radius of droplet base) and small hysteresis (i.e., $\cos\theta_R - \cos\theta_A$) are crucial for minimizing surface friction to a droplet.

22.2.3 Methodology of Measuring CA

Different ways exist in measuring wettability of a surface. An easy way is using static contact angle (simply called as contact angle in many reports) to characterize surface wettability, which is basically measured by gently putting a droplet onto a surface and then recording the acquired contact angle. The measured static contact angle does not certainly reflect the energetically most favorable state of the system; instead it may adopt any values that are allowed by energetically local minima. Another way is to characterize both the advancing and receding contact angles. For superhydrophobic/superoleophobic surfaces, one key concern is the mobility of droplets on the surface. The mobility is determined by the hysteresis effect, which is directly related to the advancing and receding contact angles. Based on the pinning force relationship in Eq. (22.5), one can quantitatively analyze that at given advancing and receding angles, a droplet of certain volume can be driven to move along a surface by its own gravity. On the other hand, merely static contact angle is not able to provide sufficient information on droplet mobility, though a high static contact angle can help reduce the solid–liquid contact area. Nor a static contact angle tells us information on whether the system is in Wenzel or Cassie state, which is also important for droplet mobility since only Cassie-type droplets are expected to be mobile on surfaces. A Wenzel-type droplet may exhibit very high advancing or static contact angles even close to 150° while at the same time showing a receding contact angle near to zero [46]. In such cases, high static contact angles give obviously

incomplete and sometimes misleading information on surface wettability since the surfaces are in fact highly sticky to droplets. In contrast, by measuring both advancing and receding contact angles, we can easily evaluate whether a surface is repellent enough to droplets, even without knowing whether the system is in Wenzel or Cassie state in advance. Therefore, we would like to emphasize here the importance of characterizing both advancing and receding contact angles in studying superhydrophobic/superoleophobic surfaces.

22.3 Nanocellulose-Based Superhydrophobic and Superoleophobic Surfaces

Aerogels are a class of highly porous and extremely lightweight materials consisting of a percolating network of solid material with 90–99% air as the matrix medium [47]. Most common aerogels are silica aerogels, though also organic aerogels and more recently cellulose-based aerogels have been made. Because aerogels have a nanorough surface, they can be made superhydrophobic when the surface is chemically modified with a surfactant. In the case of superhydrophobic silica aerogels, it is demonstrated that they have a very high contact angle not only for water [48] but also for oils, as caused by the overhang structure of the surface topography [49]. Even more, the trapped air layer combined with the aerogel's through-porous structure enables efficient underwater gas exchange [48], and nonwetting properties are damage tolerant as their self-similar network structure allows fresh reentrant surface topographies even after removal of the uppermost layer upon mechanical abrasion [49].

Cellulose aerogels are typically made from cellulose nanofibers [27, 50–62], though also regenerated cellulose [63] and cellulose nanowhiskers have been used as starting material [64]. Aerogels are usually prepared starting from the corresponding hydrogels, where the solid network is swollen in a suitable solvent. Subsequently, the solvent is removed which is a critical step as it is essential to avoid collapse and shrinkage of the network.

Simply drying of the nanocellulose hydrogels in ambient conditions does not work, as capillary forces acting between the nanofibrils will pull the nanofibrils together, resulting in a dense low-porous solid film. Care needs to be taken to avoid liquid–gas interfaces, and two approaches are very successful: supercritical drying and freeze-drying. In supercritical drying, the solvent is replaced by CO_2, which can be taken to the supercritical state at a moderate pressure and temperature. The supercritical state is a state where there are no distinct liquid and gas states, and thus also the interface between them is nonexistent. By careful control of conditions, the supercritical CO_2 can be converted to gas, resulting in the effective removal of the liquid solvent without any disturbing surface tension effects. Although supercritical dried cellulose aerogels are highly porous, there typically still is some aggregation. This is because CO_2 is insufficiently soluble in water to allow exchange directly from the hydrogel, and an intermediate organogel is needed using compatible organic solvents (e.g., ethanol). The solvent exchange from water to organic solvent and finally to CO_2 will give rise to a certain degree

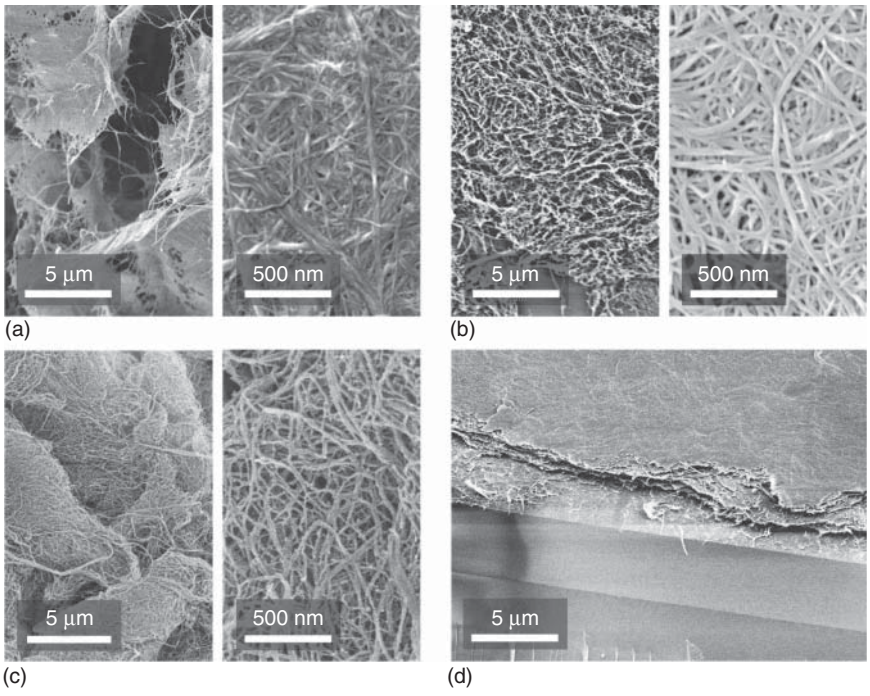

Figure 22.7 SEM images of cellulose aerogels prepared using different drying methods: (a) freeze-drying by freezing nanocellulose hydrogel in liquid nitrogen followed by sublimation of ice in vacuum leads to aerogels with sheetlike aggregates; (b) freeze-drying in liquid propane leads to a fibrillar aerogel with suppressed aggregation, provided the sample is sufficiently thin; (c) supercritical drying leads to fibrillar aerogels essentially without aggregates even in thick samples; and (d) drying in ambient conditions leads to collapse of the structure. (Korhonen *et al*. 2011 [57]. Reproduced with permission of American Chemical Society.)

of aggregation. To avoid solvent exchange, one can use freeze-drying of cellulose hydrogels, in which water is rapidly frozen followed by its removal through sublimation. Three different freeze-drying methods have been investigated, all leading to cellulose aerogels: vacuum freeze-drying, liquid nitrogen freeze-drying, and liquid propane freeze-drying (Figure 22.7). In vacuum freeze-drying, the cellulose hydrogel is placed in a vacuum chamber, and the sample cools down due to evaporation, leading to freezing. Subsequent sublimation of the ice results in an aerogel that is highly aggregated. Freezing of the hydrogel by immersion into liquid nitrogen (−196 °C) followed by sublimation leads to smaller aggregates and more fibrillar aerogels. Even less aggregated and more fibrillar aerogels were obtained by immersing the hydrogel in liquid propane that was cooled to −100 °C. The different freeze-drying methods clearly affected the aerogel structure, and it was attributed to the differences in freezing rate. Aggregation is caused by ice crystal formation that forces the cellulose fibrils to move with the ice crystal front. The voids in the aerogel are formed by the ice crystals. In the case of fast freezing with liquid propane, the ice crystals remain very small, leading to highly fibrillar

aerogels. For liquid nitrogen, freezing rate is slower as caused by the Leidenfrost effect, where a nitrogen vapor layer is shielding the liquid water in the hydrogel from the liquid nitrogen. This vapor layer presents a thermal barrier that slows down heat transfer, resulting in larger ice crystals and larger voids and more aggregation in the cellulose aerogel.

Cellulose aerogels have a nano-/microstructured rough surface topography, which is one of the requirements for making a superhydrophobic surface; however, in addition the surface needs a suitable chemical modification. After all, the cellulose surface has a high density of hydroxyl groups, making cellulose aerogels hydrophilic and absorbing water quickly. To hydrophobize the cellulose surface, three methods have been applied: carbonization, inorganic film deposition, and organic film deposition.

In carbonization, the cellulose aerogel is pyrolyzed by heating to 700–1300 °C in the absence of oxygen in an argon atmosphere, leading to the removal of all the noncarbon atoms (Figure 22.8) [65]. As a consequence, the hydroxyl groups of cellulose are removed, and carbon fibers remain. After pyrolysis, the volume of obtained carbon nanofiber aerogel is only 15% of that of the original bacterial cellulose aerogel. Meanwhile, the density decreases from 9–10 to 4–6 mg cm^{-3} for cellulose nanofibril (CNF) aerogels. The resulting material becomes black and hydrophobic with water contact angle (WCA) up to 128°, and features fire resistance, elasticity under compression, can uptake organic liquids, and has compression-dependent electric conductivity.

Also inorganic coatings on the nanofibers can hydrophobize cellulose aerogels. Atomic layer deposition (ALD) is a technique that deposits highly conformal layers of inorganics with excellent nanometer control on the deposited thickness [66]. Using ALD, cellulose aerogels have been coated with Al_2O_3, ZnO, and TiO_2, and the deposited film thickness is uniform throughout the whole sample (Figure 22.9) [57]. By heating, the cellulose can be removed to obtain a hollow nanotube aerogel, where the thin inorganic coating is sufficiently strong to preserve the aerogel structure. This nanotube aerogel can function as a resistive humidity sensor with fast response. The TiO_2 coating on the cellulose aerogel also provides photoswitchable wetting properties [59]. The TiO_2-coated aerogel is hydrophobic with contact angle of 140° and does not absorb water. By UV illumination, the aerogel becomes a superabsorbent for water (absorbing 16 times its own weight), as demonstrated by a vanishing contact angle. The original absorption and wetting properties slowly recover upon storage in the dark. The same type of TiO_2-coated cellulose aerogel can also be used as oil-absorbent material [56]. The water repellency and its low density enable the aerogel to easily float on the water surface. On the other hand, the oleophilic surface and the open porous structure allow the aerogel to easily absorb nonpolar liquids and oils up to nearly all of its initial volume, which allows it to collect organic contaminants from the water surface. The materials can be reused after washing, recycled, or incinerated with the absorbed oil. The cellulose is renewable and titanium dioxide is not environmentally hazardous, thus promoting potential in environmental applications.

When the cellulose nanofibers are modified with a surfactant, the cellulose aerogel becomes superhydrophobic and oleophilic in the case of alkyl surfactants [60] and even superoleophobic in the case of fluorinated surfactants [54, 55].

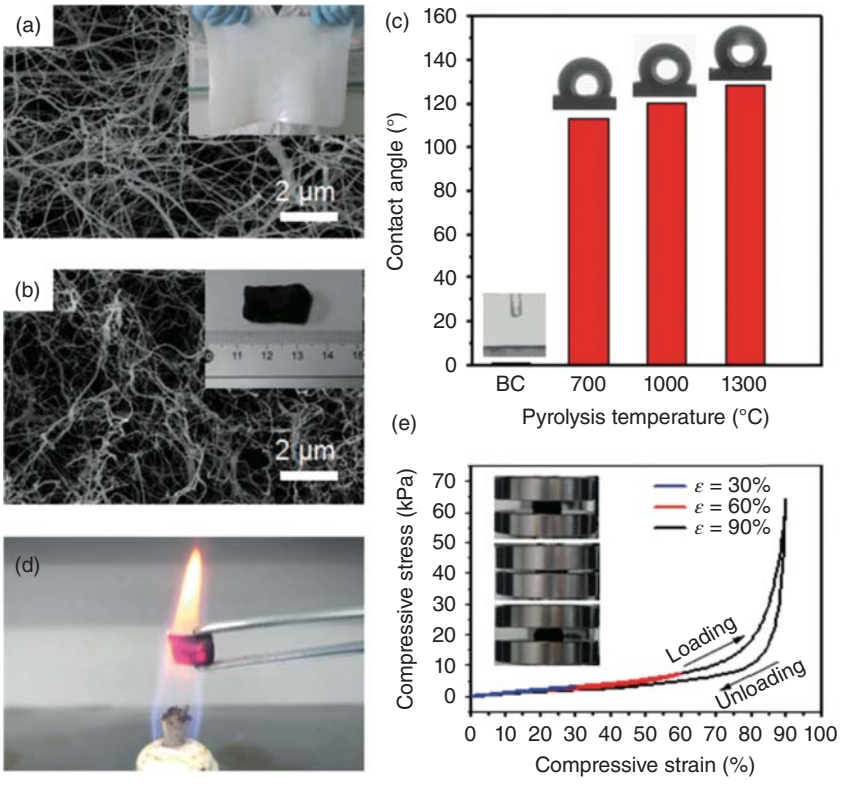

Figure 22.8 (a,b) SEM images of the bacterial cellulose aerogel (a) and the carbon nanofiber aerogel treated at 1300 °C (b). The insets in (a) and (b) show the photographs of the bacterial cellulose pellicle and the CNF aerogel prepared by pyrolysis at 1300 °C. (c) Water contact angle measurements of the original cellulose aerogel and the carbon nanofiber aerogels prepared by pyrolysis at different temperatures, indicating that the hydrophobic properties of carbon nanofiber aerogels improved with increasing pyrolysis temperature. (d) Photograph of carbon nanofiber aerogel in a hot flame of an alcohol burner. (e) Compressive stress–strain curves of a carbon nanofiber aerogel at different set strains ε of 30%, 60%, and 90%. The inset in (e) shows the sequential photographs of the carbon nanofiber aerogel during the compression process (in the middle, the compressed form is shown). (Wu *et al*. 2013 [65]. Reproduced with permission of John Wiley & Sons.)

One type of fluorinated surfactant is (tridecafluoro-1,1,2,2-tetrahydrooctyl) trichlorosilane, which can anchor to the cellulose surface by reaction of the trichlorosilane group to the surface hydroxyl. These aerogels not only repel water and oil droplets; in addition they also support considerable load on a water/oil surface as inspired by flotation of insects on water due to their superhydrophobic legs and exhibit reduced viscous drag (Figure 22.10A) [54]. The aerogel is capable of supporting a weight nearly 3 orders of magnitude larger than the weight of the aerogel itself (Figure 22.10B). The load support is achieved by surface tension acting at different length scales: at the macroscopic scale along the perimeter of the carrier and at the microscopic scale along the cellulose nanofibers by preventing soaking of the aerogel, thus ensuring buoyancy [69].

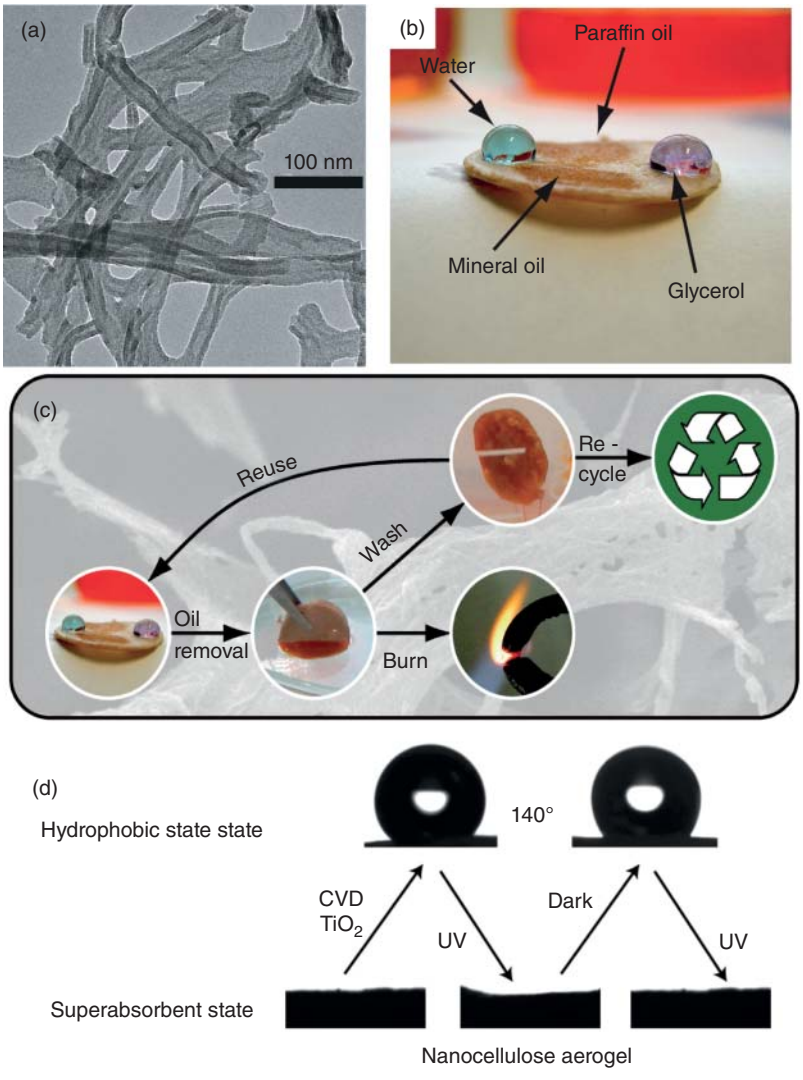

Figure 22.9 (a) TEM image of TiO_2-coated nanocellulose aerogel, showing conformal TiO_2 layers. (Adapted from Kettunen *et al*. 2011 [59]. Reproduced with permission of American Chemical Society.) (b) TiO_2-coated aerogels are hydrophobic and oleophilic: the water and glycerol stay as droplets (colored with dyes), whereas paraffin oil and mineral oil are readily absorbed. (c) The TiO_2-coated aerogel acts as an oil absorbent, able to collect organic contaminants from the water surface. The materials can be reused after washing, recycled, or incinerated with the absorbed oil. (Adapted from Korhonen *et al*. 2011 [56]. Reproduced with permission of American Chemical Society.) (d) Switchable absorption and wetting upon TiO_2 coating of the nanocellulose aerogel and the effect of UV illumination. (Adapted from Kettunen 2013 [67]. Reproduced with permission of John Wiley & Sons.)

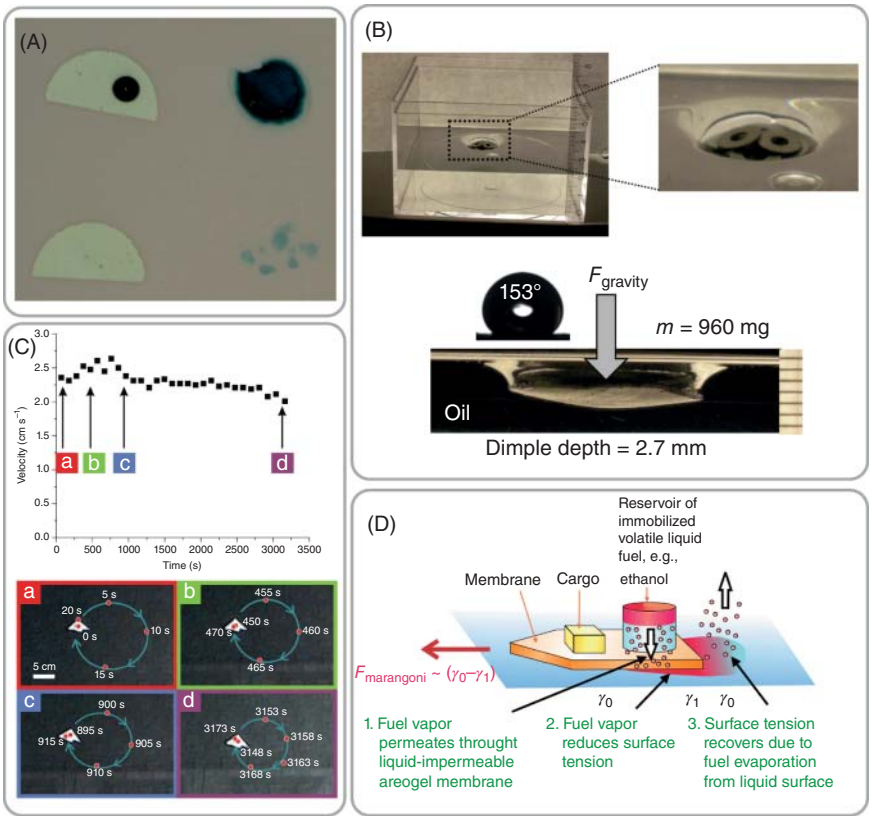

Figure 22.10 (A) A drop of ink spreads rapidly on unmodified nonfluorinated aerogel (top right) and washing in water does not remove the color, but the nonfluorinated aerogel disintegrates instead (bottom right). In contrast, ink forms a round drop on fluorinated aerogel membrane (top left), and it can be easily washed away using water, demonstrating dirt repellency (bottom left). (B) Contact angle measurement and load-carrying experiment of the aerogel on paraffin oil. The side-view photograph of the aerogel load carrier on paraffin oil shows the dimple at maximum supportable weight. (C + D) Steady-velocity locomotion on water based on nanostructured superhydrophobic and superoleophobic aerogel membranes with onboard ethanol as fuel. (Adapted from Jin *et al*. 2011 [54] and Jin *et al*. 2012 [68]. Reproduced with permission of American Chemical Society and Royal Society of Chemistry.)

The aerogels are gas permeable due to their open porous nanofibrillar structure and float on water and oils due to their superhydrophobic and superoleophobic nature. A continuous, prolonged, and tunable motion of the floating aerogel was achieved by a vapor-driven Marangoni propulsion(Figure 22.10(C + D)) [68]. A very small amount of onboard fuel (i.e., 25 µl of ethanol) allowed autonomous steady-velocity locomotion at a range of 74 m during nearly 1 h for a centimeter-sized object. The steady velocity is achieved through a continuous supply of fuel vapor that lowers the surface tension of the liquid, combined with the spontaneous recovery of the surface tension after the floating machine has passed.

Researchers recently introduced a simple route for the esterification and processing of CNFs (or nanopaper) with the aim of reducing their hydrophilicity and producing hydrophobic cellulose nanopaper with reduced moisture sensitivity [70]. The preparation steps of hydrophobic nanopapers involved vacuum filtration, solvent exchange from water to acetone, and reaction with anhydride molecules bearing different hydrophobic alkyl chains by hot pressing. Porous films having a surface area between 38 and 47 g m^{-2} and pore sizes in the 3–200 nm range were fabricated (Figure 22.11). This method preserved the crystalline structure of native cellulose and successfully introduces hydrophobic moieties on CNF surface as confirmed by FTIR, XPS, and elemental analysis. As a result, modified nanopapers were demonstrated to have a reduced moisture uptake, higher surface WCA, and wet tensile properties as compared with reference nonmodified nanopaper, thus illustrating the benefit of the modification for the use of cellulose nanopaper in humid environments.

As an alternative approach, native wood celluloses can be converted to individual nanofibers 3–4 nm wide that are at least several microns in length, that is, with aspect ratios >100 (Figure 22.12a), by (2,2,6,6-tetramethylpiperidine-1-oxyl) (TEMPO) radical-mediated oxidation and successive mild disintegration in water [71]. These nanostructured cellulose materials are known as 2,2,6,6-tetramethylpiperidine-1-oxyl-oxidized cellulose nanomaterial (TOCN). Self-standing films with sufficient light transparency and flexibility were prepared from softwood and hardwood TOCN/water dispersions. The densities and moisture contents of TOCN films conditioned at 22 °C and 50% relative humidity were approximately 1.45–1.47 g cm^3 and 13–15%, respectively. The tensile strengths and elastic moduli of the films were 200–300 MPa and 6–7 GPa, respectively, which were higher than those of cellophane films. The highly hydrophilic nature of TOCN films leads in turn to low contact resistance to water (Figure 22.12b). The contact angle of a water droplet placed on a TOCN film decreased from 47° over time as a result of partial penetration of water into the film. Alkyl ketene dimer (AKD) is a typical hydrophobizing

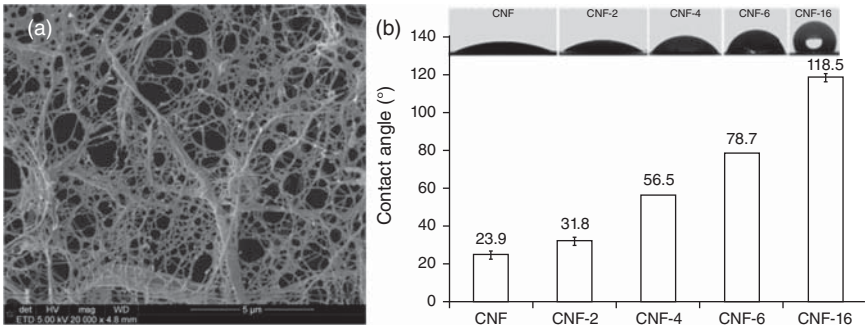

Figure 22.11 (a) SEM image of unmodified CNF. (b) Static water contact angle for reference and esterified nanopapers. Esterified nanopapers have been denoted CNF-N where *N* represents the number of carbon in the grafted entity. In this nomenclature, *N* is equal to 2, 4, 6, and 16 for the esterification with acetic, butyric, hexanoic, and 2-dodecen-1-yl-succinic anhydrides, respectively. (Sehaqui *et al*. 2013 [70]. Reproduced with permission Springer.)

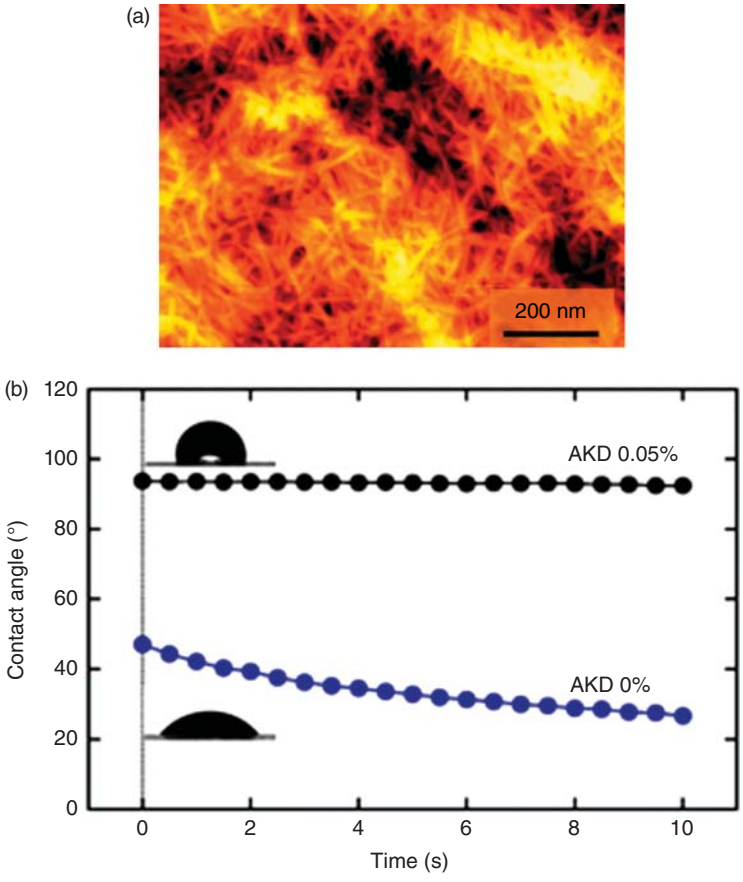

Figure 22.12 (a) AFM image of the surface of a nanofiber film prepared from TEMPO-oxidized softwood cellulose. (b) Change in the contact angle over time of a water droplet on a nanofiber film prepared from TEMPO-oxidized softwood cellulose before and after treatment with a 0.05% alkyl ketene dimer dispersion. (Isogai *et al*. 2011 [71]. Reproduced with permission of Royal Society of Chemisrty.)

chemical used in papermaking processes. TOCN film treated with a 0.05% AKD dispersion had a WCA of 94°, and this value was maintained for 10 s. Therefore, hydrophilic TOCN films can be hydrophobized using a simple soaking method with a cationic AKD dispersion (Figure 22.12b). The abundant carboxylate groups in the TOCN film are likely to behave as adsorption sites for cationic AKD-dispersed particles.

AKD agent is commonly used in sizing of hydrophobic paper. It can also be used to treat the surfaces of nanostructured cellulose in order to increase hydrophobicity. Researchers have implemented this process in fabricating liquid-repellent nanocellulose coatings on paper [72]. This can be done via a facile two-step dip coating method. In the first step, filter paper samples were dip-coated using an aqueous suspension containing precipitated calcium carbonate (PCC) pigments and cellulose nanofibers to form a highly rough

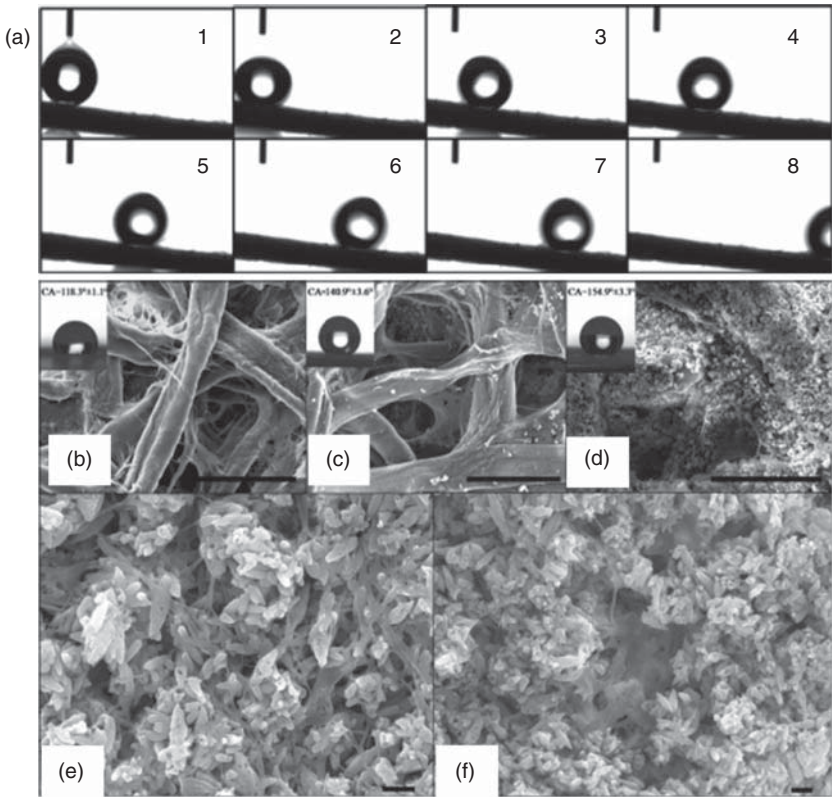

Figure 22.13 (a) The water rolling-off angle: Figures (1–8) are video frames of a 5 μl water droplet being placed on the tilted (5°) surface of superhydrophobic paper. The composition of the superhydrophobic coating layer was 100 g PCC:5 g cellulose nanofibers. The water droplet began to roll off the superhydrophobic paper surface as the tilting angle of the surface increased to 5°. SEM images of (b) AKD-sized filter paper (scale bar = 50 μm); (c) filter paper dip-coated with PCC without using cellulose nanofibers as binder and then sized with AKD (scale bar = 50 μm); (d) filter paper dip-coated with PCC with added cellulose nanofibers as binder and then sized with AKD subsequently (scale bar = 50 μm); (e) the interaction between PCC particles and cellulose nanofibers when the slurry was coated on a glass slide (scale bar = 1 μm); and (f) cellulose nanofibers and nano- and microfilm patches of the recombined nanofibers connecting and holding the PCC particles together (scale bar = 1 μm). (Arbatan *et al*. 2012 [72]. Reproduced with permission of Elsevier.)

layer on the surface of the filter paper. Subsequently, the coated papers were treated with a solution of AKD in *n*-heptane, which led to the formation of superhydrophobic paper (Figure 22.13a). Contact angle measurements confirmed the superhydrophobic nature of the paper prepared. SEM analysis was also carried out to characterize the surface differences of the coated paper samples with and without the added cellulose nanofibers to clarify the binding role of cellulose nanofibers (Figure 22.13b–e). It was observed that cellulose nanofiber is a critical component to the formation of the rough PCC coating layer required for giving superhydrophobicity; it significantly improves the retention of PCC clusters on the surface of the paper, and the retained PCC

clusters offer the structure of dual-scale roughness. It should be noted that AKD only contributes to the surface hydrophobicity, but not to the surface roughness. Such simple, fast, and cost-effective fabrication method may lead to further development in production and application of superhydrophobic papers treated with nanocellulose or nanocellulose composites.

Robust, superhydrophobic, and self-cleaning films were also fabricated using nano- or microstructured cellulose fatty acid esters, which were prepared via nanoprecipitation process [73–75]. The superhydrophobic films could be coated on diverse surfaces with nonuniform shapes by distinct coating techniques. The superhydrophobic films could be spray-coated on objects with hydrophilic or hydrophobic surfaces and with nonuniform shapes, such as a metal spoon, a plastic fork with curved surfaces, or a piece of textile fabric with many small fibers at its surface (Figure 22.14a–d). These superhydrophobic films were found to be stable under normal conditions in air for more than 2 months or under water for at least 96 h. Nanostructured films required a thickness of at least 1 μm to become superhydrophobic, while nano-/microstructured films required a thickness of more than 10 μm. Due to the low amount of required cellulose esters, the films were semitransparent. Figure 22.14 further shows that superhydrophobic films could be regenerated on-site after mechanical damages, for example, by scratching or by a high-temperature treatment. In comparison, most known superhydrophobic surfaces had limited possibility to be regenerated on damaged spots or required particular processing conditions, such as high temperature or special equipment.

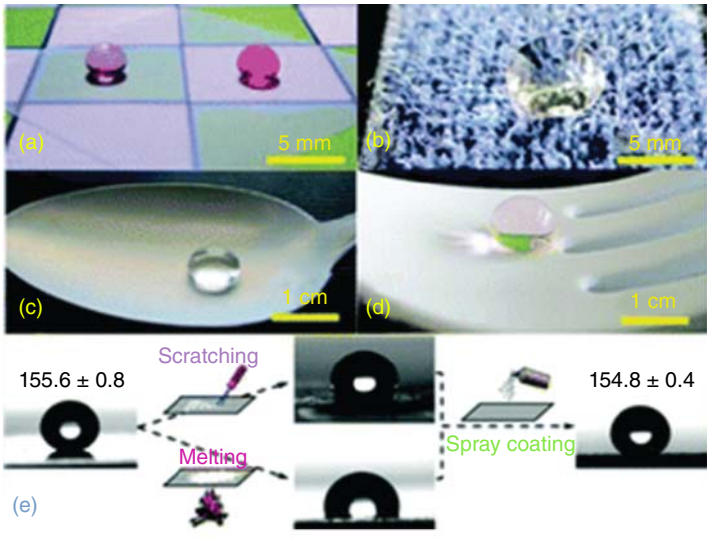

Figure 22.14 Superhydrophobization of various surfaces by the deposition of cellulose ester nanoparticles via spray coating. (a) Glass; (b) cloth textile; (c) metal spoon; or (d) plastic fork. Red and pink colors are due to dissolved dye in water for better visualization. Scale bar in (a/b): 5 mm and in (c/d): 1 cm. (e) Regeneration of damaged superhydrophobic films (by scratching or melting at high temperature) via on-site spray coating. (Geissler *et al*. 2013 [73]. Reproduced with permission of Royal Society of Chemisrty.)

Electrospinning is a highly versatile method for producing fibers with fiber sizes ranging from low micron to hundreds of nanometers. The fibers are spun or deposited from polymer solutions as nonwoven mats with important properties such as high surface-to-volume ratio, high porosities, small pore sizes, and high possibility to blend in nanostructured fillers. Flexibility of the process allows for the creation of fibers with various submicron morphologies, such as round, flat, smooth, and beaded.

Cellulose triacetate (CTA) has been widely used in membrane technology because it has good hydrolytic stability and excellent resistance to free chlorine and biodegradation. Nano-/microfibrous CTA mats were prepared by electrospinning a fixed concentration of CTA with different methylene chloride/ethanol (MC/EtOH) ratios and with various concentrations of CTA at a fixed MC/EtOH 80/20 (v/v) ratio [76]. All of the electrospun CTA mats had a high WCA compared to the CTA cast film. At a solvent composition of 80/20 (v/v) and 5 wt% CTA concentration, the CTA mat without plasma treatment had good surface roughness and electrospinning processability (Figure 22.15), and its WCA was 142°. To further improve its hydrophobicity, the CTA fibrous mat electrospun from the 5 wt% solution of CTA was treated with a CF_4 plasma for various times. Superhydrophobicity could be obtained after the CF_4 plasma treatment. The WCA of the CTA mat reached as high as 153° after plasma treatment for 60 s. After plasma treatment for 60 s, the WCA and WTA of the CTA fibrous mat reached as high as 153° and as low as 4°, respectively, indicating

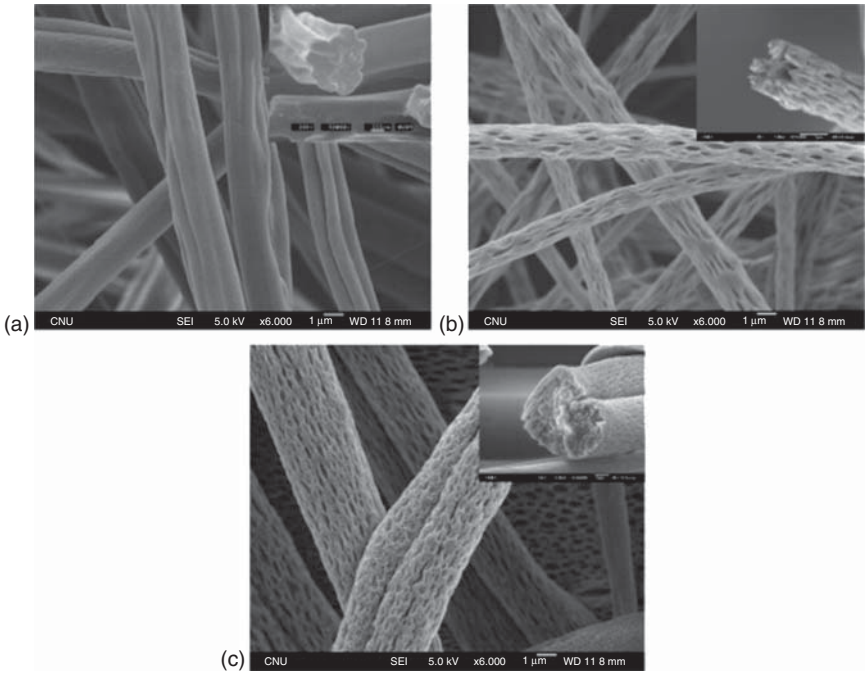

Figure 22.15 SEM images of CTA fibers electrospun with different MC/EtOH (v/v) ratios; (a) 80/20, (b) 90/10, and (c) 100/0. (Yoon *et al*. 2009 [76]. Reproduced with permission of Elsevier.)

that the CTA surface is superhydrophobic. Further plasma treatment reduced the surface roughness of the CTA mat, thus decreasing its WCA. The extremely high hydrophobicity of the CTA fibrous mat after plasma treatment for 60 s was attributed to the inherent surface roughness and surface fluorination.

It is also possible to form nanofibers on microfibers in order to induce a hierarchical texture. In doing so, the higher mechanical strength of the microfiber is combined with the large surface area of the electrospun nanofibers. Such nanofiber-coated microfibers find use in many different applications such as tissue engineering scaffolds to create porous structures where porosity as well as other material properties may be well controlled and tailored to best promote and support cell growth [77]. There are also ample possibilities for nanofiber-coated microfibers within smart textiles, where the composite structure of the nanofiber-coated microfiber allows for many options in terms of material choice, and the ample possibilities of incorporating particles are also advantageous.

The nanofiber coating creates a rough surface structure. As stated by Cassie and Baxter, this is one important feature for the creation of a hydrophobic surface. The other important feature for creation of a superhydrophobic surface is that of a low surface energy. In Figure 22.16, an example of nanofiber-coated microfibers (regenerated) plasma-treated with trifluoromethane to achieve desired surface chemistry is shown. Successful deposition of fluorine was confirmed by *in situ* X-ray diffraction measurements, the atomic concentration on the measured surface reaching 7.7% F on the noncoated microfiber and 12.2% and 14% F on the regenerated and nonregenerated nanofiber-coated microfibers, respectively. According to the authors, it was found that noticeably more fluorine was deposited on microfibers coated with nanofibers compared with noncoated microfibers. This difference was attributed to the higher available surface area provided by the nanofiber coating and highlights the advantage of

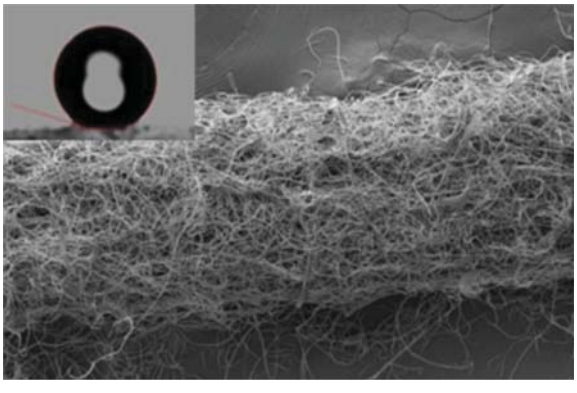

Figure 22.16 SEM image of a Lyocell™ filament microfiber decorated with CA nanofibers. A cellulose microfiber coated with cellulose nanofibers, which after plasma treatment exhibit superhydrophobic character. The inset shows a drop of water on the fiber surface, illustrating the hydrophobicity of the material. (Thorvaldsson *et al*. 2012 [77]. Reproduced with permission Springer.)

using nanostructures in surface modification processes. Also, no morphological changes were seen upon SEM analysis of the plasma-treated fibers.

Very recently, electrospun nanofiber mats containing cellulose were used as templates with water-triggered modulus changing hydrophobic nanocomposites [78]. More specifically, biomimetic stimuli-responsive nanocomposites were made using two rubbery polymers as the waterproof layer, low-modulus matrix and hydrophilic cellulose whiskers as the high-modulus filler, and texture and roughness enhancer in order to enhance degree of hydrophobicity. These materials were prepared using a template approach, which involves the formation of a percolating cellulose whisker network, and filling this template with either of the matrix polymers (Figure 22.17). Dynamic mechanical analysis (DMA) studies of the dry nanocomposite films revealed that the incorporation of cellulose whiskers into the rubbery polymers increased the tensile storage modulus significantly. The reinforcement was attributed to the formation of a three-dimensional (3D) network within the rubbery matrices. The incorporation of the cellulose whiskers did not affect the main relaxation temperature of the matrix rubber polymer, suggesting weak nanofiller–polymer interactions. Thus, the reinforcement is primarily on account of the nanofiller–nanofiller interactions, which involve hydrogen bonding. More importantly, submersion of these hydrophobic matrix cellulose nanowhisker nanocomposites in water results in dramatic softening, consistent with disengagement of the cellulose nanowhisker network as a consequence of competitive hydrogen bonding with water. Given the hydrophobic nature of the matrices, it was proposed that the cellulose nanowhiskers create a percolating network of hydrophilic channels within the hydrophobic rubbery polymer. As such, this type of behavior suggests the potential of such films to be used as the basis of selective membranes.

ZnO-embedded nanostructured cellulose acetate (CA) fibrous membranes had been prepared by electrospinning from solution [79]. It was found via detailed

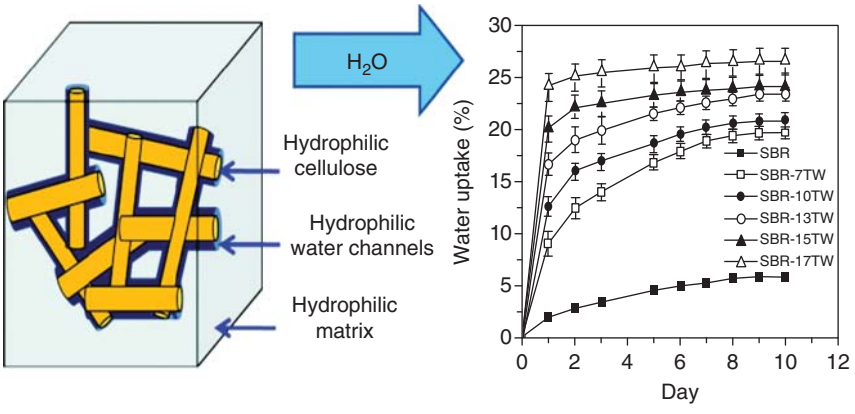

Figure 22.17 Schematic representation of the mechanism for water transport and swelling of cellulose nanocomposites and the effect of cellulose nanowhisker concentration on the water uptake properties. SBR represents the rubber polymer and TW stands for cellulose nanowhiskers isolated from tunicates; for further details see [78].

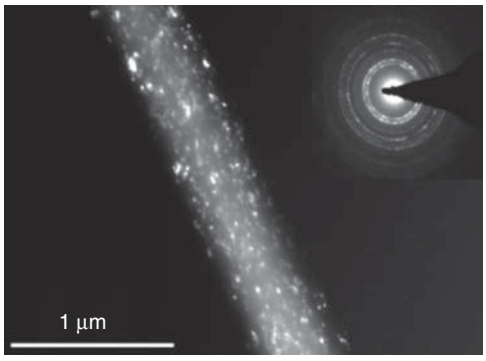

Figure 22.18 Cellulose acetate nanofibers decorated with ZnO nanoparticles obtained as a result of electrospinning from solution. (Anitha *et al*. 2013 [79]. Reproduced with permission of Elsevier.)

FTIR analysis that ZnO and CA formed hydrogen bonds. The ZnO-embedded fibrous membranes showed a higher degree of water repellency than pure CA membrane. The sample exhibited strong antibacterial activity against *Staphylococcus aureus*, *Escherichia coli*, and *Citrobacter*. Moreover, the wettability of the surfaces could be tuned from hydrophilic to hydrophobic. This effective, rapid, and simple method provided a new approach to fabricate the hydrophobic surface without the need for further surface treatment (Figure 22.18). Therefore, the electrospinning technique is still considered as one of the best procedures for the synthesis of composite fibrous nanostructured cellulose membranes, since agglomeration of nanoparticles is prevented and the contact area between the surface and the microorganisms is increased.

Development of robust liquid-repellent surfaces using cellulosic materials via simple fabrication methods is of fundamental interest for research and industrial applications. Recently researchers have reported a simple, fast, and reproducible method that could easily be scalable to large and irregular areas for fabricating transparent slippery surfaces based on nanoporous films of sustainable cellulose lauroyl ester (CLE) via spray coating (Figure 22.19). These slippery surfaces were liquid repellent for water, ionic liquids, and some organic liquids such as glycerol [80]. Furthermore, the work also showed excellent liquid repellency upon liquid impact and outstanding anti-icing properties. Their small contact angle hysteresis and low adhesion enabled the 3D manipulation of drops by applying external magnetic forces. In addition, the fabrication of slippery surfaces using CLE is not limited by the size or the geometry of the surface because spray coating is a very generally applicable coating technique.

Since CLE is not a common cellulose derivative, it is important to briefly describe its synthesis. In a typical case, 1 g of cellulose powder was washed with methanol and pyridine to remove traces of moisture before it was suspended in 30 ml of pyridine. Under stirring, the mixture was heated to 100 °C. Then, 8.96 ml of lauroyl chloride (98%) (2 mol per mol OH of cellulose) was dropped to the hot suspension while the system was purged with nitrogen. After 1 h of stirring at 100 °C, the reaction mixture was poured (still hot) into 200 ml of ethanol, and the precipitate was separated by centrifugation. The product was purified via repeating dissolution in dichloromethane and precipitation in five volumes of ethanol. Lastly, the product was dried under vacuum. Such cellulosic transparent

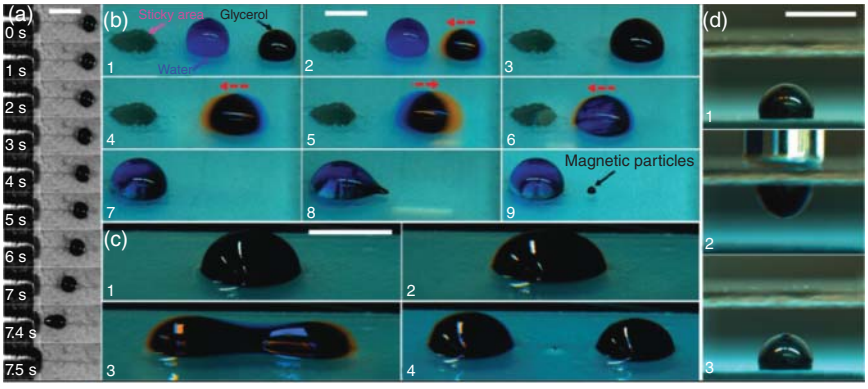

Figure 22.19 (a) Horizontal movement of a 25 μl magnetic glycerol drop by a normal magnet (the magnet is on the left). The magnetic field is 0.06 T. The scale bar is 10 mm. (b) Magnetic glycerol drop (25 μl) moved by the magnetic field to a 30 μl water drop. After coalescing, the two liquids were mixed by "shaking" the drops, and the mixed drop was moved to a sticky area. Eventually, the magnetic particles were removed from the mixed drop by the magnet. (c) Magnetic glycerol drop (60 μl) divided into two droplets by two magnets applied beside the drop. (d) Magnetic glycerol drop (15 μl) transferred from a lower to an upper surface and back by a moving magnet. The scale bar in (b–d) is 5 mm. (Chen *et al*. 2014 [80]. Reproduced with permission of American Chemical Society.)

and nanostructured slippery substrates were fabricated by spray-coating nanoparticle suspensions of sustainable CLE that were subsequently infused with a perfluorinated lubrication liquid [80].

The slippery CLE films exhibited very low adhesion for static and dynamic wetting processes and also showed good anti-icing properties by significantly retarding the ice formation process at −10 °C under ambient conditions. The low adhesion and friction between the coating and various liquids enable 3D drop manipulation via magnetic actuation, as required for open microfluidic applications. These CLE films were considered promising for use in many applications such as the coating of car windows, solar cell panels, and microfluidic devices.

Nanofibrillated cellulose (NFC) refers to cellulose fibers that have been fibrillated to achieve agglomerates of cellulose microfibril units; NFCs have nanoscale (less than 100 nm) diameter and typical length of several micrometers. Several denominations exist for describing such material, and most often nanofibrillated cellulose/microfibrillated cellulose (NFC/MFC) is used [81]. Two approaches were employed for preparing superhydrophobic surfaces using NFC [82]. The first approach consisted of applying the NFCs to a substrate, followed by a gas-phase coating with a fluorine-containing trichlorosilane surfactant via chemical vapor deposition, and the second approach included hydrophobization of the NFCs in a solution with the fluorinated trichlorosilane surfactant, followed by coating the NFCs onto the substrate (Figure 22.20a,b). Both methods resulted in superhydrophobic surfaces, as determined by contact angle measurements and observation of reflection when immersed in water (Figure 22.20c). Importantly, sliding angles of only a few degrees were recorded from both methods, which potentially enable self-cleaning applications. In addition, liquid marbles

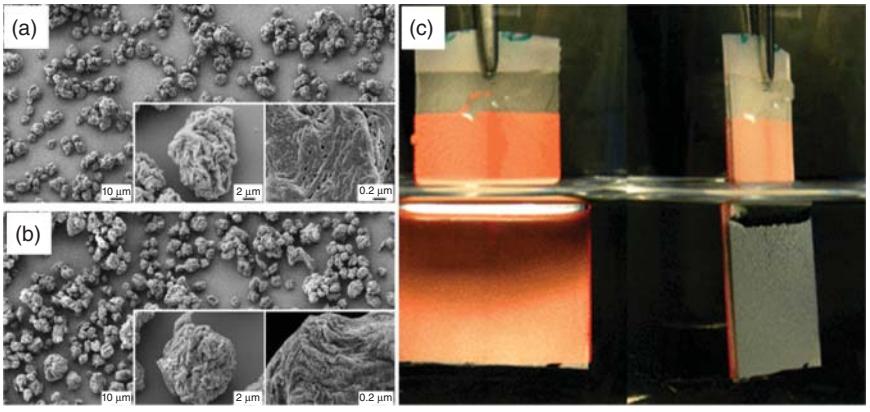

Figure 22.20 (a) Surface structures of a sample with spray-dried NFC microparticles by approach A before fluorination. (b) A sample with fluorinated NFC microparticles, prepared by approach B. (c) A glass slide of fluorinated NFC microparticles, prepared using approach A, immersed in water. When viewed beyond the critical angle, a total internal reflection can be observed, implying the presence of the plastron and thus superhydrophobicity. Orange paper was attached at the backside of the sample in order to facilitate observation of the reflection. (Mertaniemi *et al*. 2012 [82]. Reproduced with permission of Royal Society of Chemistry.)

were prepared using hydrophobic cellulose particles prepared by the second approach. The surface pattern achieved by depositing the spray-dried NFC microparticles on surfaces was observed to have hierarchical roughness qualitatively similar to lotus leaves. Furthermore, spray-dried NFC microparticles are particularly attractive for preparing superhydrophobic surfaces, since cellulose is a cheap natural product available in large amounts and spray drying of cellulose nanofibers is an industrially feasible process.

One of the first studies on superhydrophobic cellulose nanocomposites was achieved using cellulose nitrate. Cellulose nitrate was rendered self-cleaning superhydrophobic by blending with natural rubber and clay nanoparticles using a multicomponent solvent system [83].

It was a simple spray coating technique to fabricate rubber-toughened cellulose/organoclay nanocomposite coatings with highly water-repellent surface wetting characteristics and strong adhesion to metal surfaces. The technique combined the principles of phase inversion and atomization of multicomponent cellulose nitrate/organoclay suspensions containing a biolubricant as the nonsolvent. The biolubricant was a blend of cyclomethicone/dimethiconol oil with fruit kernel oils. The ternary system of cellulose nitrate/solvent/biolubricant was blended with rubber-dispersed organoclay nanofluids. Natural, synthetic, and fluoroacrylic latex rubbers were used for the purpose. Self-cleaning superhydrophobic coatings were obtained from synthetic and fluoroacrylic rubbers, whereas natural rubber containing formulations resulted in sticky superhydrophobic coatings (Figure 22.21). The authors concluded that the hierarchical surface roughness was due to the collective formation of roughness from solution inverted cellulose nitrate morphology and embedded exfoliated clay platelets. Natural rubber compounded composites showed sticky superhydrophobic

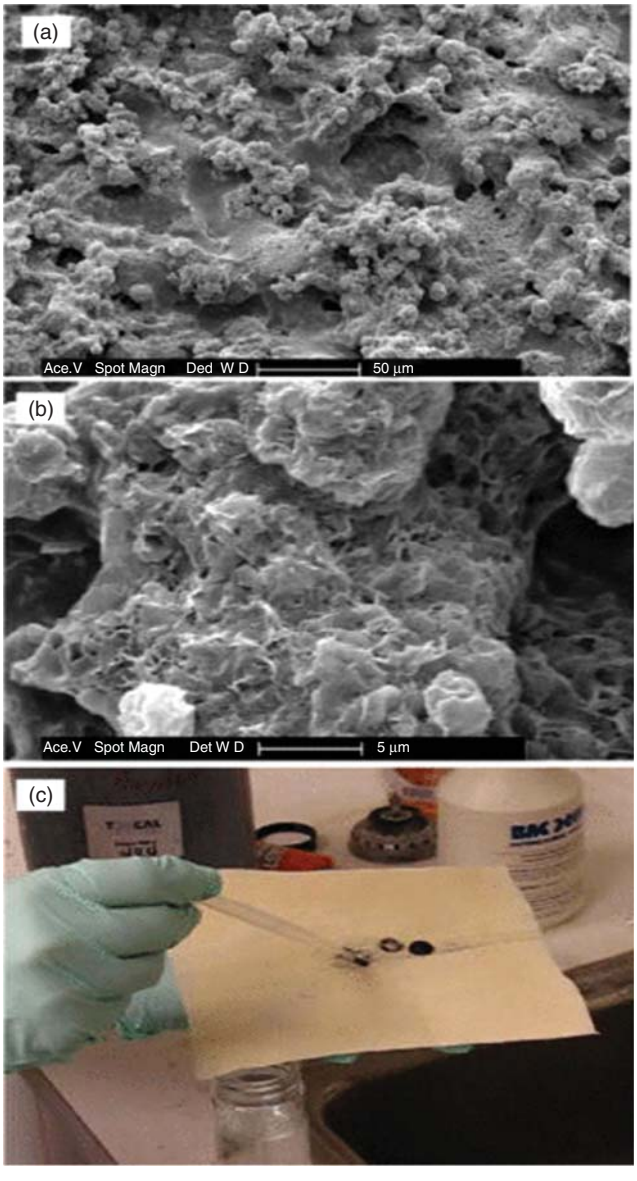

Figure 22.21 SEM images (a) and (b) showing surface morphology of the fluoroacrylic latex-reinforced superhydrophobic biopolymer–clay nanocomposite coatings. (c) Demonstration of the self-cleaning process using carbon black powder to simulate contaminated nanocomposite surfaces. (Bayer *et al*. 2009 [83]. Reproduced with permission of American Institute of Physics.)

wetting behavior. Coatings had good adhesion to aluminum metal surfaces and were proposed to be considered for various biomedical applications [83].

22.4 Summary

In short, the works presented in this chapter indicate that being able to duplicate nanostructured natural surfaces is quite commonplace now with state-of-the-art microfabrication techniques, but fabrication of liquid-repellent materials *made up of* cellulose or cellulose derivatives is still quite challenging. Review of the literature clearly shows that in one way or the other, a certain synthetic hydrophobic agent is needed even if cellulose is used in the right nanostructured form or fibers or with added surface roughness. However, there are many inspiring new ways to make functional liquid-repellent materials from cellulose and derivatives, and various practical applications have been demonstrated such as robust aerogels, oil–water separation, tuning of drug delivery rates, and so on. Use of nontoxic hydrophobic polymers and elastomers along with cellulose could be one interesting future direction as such polymers do not pose alarming environmental concerns related to C-8 fluorocompounds.

Acknowledgments

This work was supported by the Academy of Finland through its Centres of Excellence Programme (2014–2019) and under project nos. 263560, 283210 and 295005.

References

1 Xia, F. and Jiang, L. (2008) Bio-inspired, smart, multiscale interfacial materials. *Adv. Mater.*, **20** (15), 2842–2858.
2 Solga, A., Cerman, Z., Striffler, B.F., Spaeth, M., and Barthlott, W. (2007) The dream of staying clean: lotus and biomimetic surfaces. *Bioinspiration Biomimetics*, **2** (4), S126–S134.
3 Quéré, D. (2008) Wetting and roughness. *Annu. Rev. Mater. Res.*, **38** (1), 71–99.
4 Marmur, A. (2013) Superhydrophobic and superhydrophobic surfaces: from understanding non-wettability to design considerations. *Soft Matter*, **9** (33), 7900–7904.
5 Tian, Y., Su, B., and Jiang, L. (2014) Interfacial material system exhibiting superwettability. *Adv. Mater.*, **26** (40), 6872–6897.
6 Verho, T., Bower, C., Andrew, P., Franssila, S., Ikkala, O., and Ras, R.H.A. (2011) Mechanically durable superhydrophobic surfaces. *Adv. Mater.*, **23** (5), 673–678.
7 Liu, K. and Jiang, L. (2012) Bio-inspired self-cleaning surfaces. *Annu. Rev. Mater. Res.*, **42** (1), 231–263.

8 Lv, J., Song, Y., Jiang, L., and Wang, J. (2014) Bio-inspired strategies for anti-icing. *ACS Nano*, **8** (4), 3152–3169.

9 Barthlott, W. and Neinhuis, C. (1997) Purity of the sacred lotus, or escape from contamination in biological surfaces. *Planta*, **202** (1), 1–8.

10 Darmanin, T. and Guittard, F. (2015) Superhydrophobic and superoleophobic properties in nature. *Mater. Today*, **18** (5), 273–285.

11 Wong, T.S., Sun, T., Feng, L., and Aizenberg, J. (2013) Interfacial materials with special wettability. *MRS Bull.*, **38** (05), 366–371.

12 Koch, K. and Barthlott, W. (2009) Superhydrophobic and superhydrophilic plant surfaces: an inspiration for biomimetic materials. *Philos. Trans. R. Soc. London, Ser. A*, **367** (1893), 1487–1509.

13 Neinhuis, C. and Barthlott, W. (1997) Characterization and distribution of water-repellent, self-cleaning plant surfaces. *Ann. Bot.*, **79** (6), 667–677.

14 Klemm, D., Kramer, F., Moritz, S., Lindström, T., Ankerfors, M., Gray, D., and Dorris, A. (2011) Nanocelluloses: a new family of nature-based materials. *Angew. Chem. Int. Ed.*, **50** (24), 5438–5466.

15 Habibi, Y., Lucia, L.A., and Rojas, O.J. (2010) Cellulose nanocrystals: chemistry, self-assembly, and applications. *Chem. Rev.*, **110** (6), 3479–3500.

16 Eichhorn, S.J. (2011) Cellulose nanowhiskers: promising materials for advanced applications. *Soft Matter*, **7** (2), 303–315.

17 Eichhorn, S.J., Dufresne, A., Aranguren, M., Marcovich, N.E., Capadona, J.R., Rowan, S.J., Weder, C., Thielemans, W., Roman, M., Renneckar, S., and Gindl, W. (2010) Review: current international research into cellulose nanofibres and nanocomposites. *J. Mater. Sci.*, **45** (1), 1–33.

18 Moon, R.J., Martini, A., Nairn, J., Simonsen, J., and Youngblood, J. (2011) Cellulose nanomaterials review: structure, properties and nanocomposites. *Chem. Soc. Rev.*, **40** (7), 3941.

19 Lavoine, N., Desloges, I., Dufresne, A., and Bras, J. (2012) Microfibrillated cellulose – its barrier properties and applications in cellulosic materials: a review. *Carbohydr. Polym.*, **90** (2), 735–764.

20 Siró, I. and Plackett, D. (2010) Microfibrillated cellulose and new nanocomposite materials: a review. *Cellulose*, **17** (3), 459–494.

21 Mariano, M., Kissi, E.N., and Dufresne, A. (2014) Cellulose nanocrystals and related nanocomposites: review of some properties and challenges. *J. Polym. Sci., Part B: Polym. Phys.*, **52** (12), 791–806.

22 Siqueira, G., Bras, J., and Dufresne, A. (2010) Cellulosic bionanocomposites: a review of preparation, properties and applications. *Polymers*, **2** (4), 728–765.

23 Visakh, P.M., Thomas, S., Oksman, K., and Mathew, A.P. (2011) Cellulose nanofibres and cellulose nanowhiskers based natural rubber composites: diffusion, sorption, and permeation of aromatic organic solvents. *J. Appl. Polym. Sci.*, **124** (2), 1614–1623.

24 Cunha, A.G. and Gandini, A. (2010) Turning polysaccharides into hydrophobic materials: a critical review. Part 1. Cellulose. *Cellulose*, **17** (5), 875–889.

25 Salas, C., Nypelö, T., Rodriguez-Abreu, C., Carrillo, C., and Rojas, O.J. (2014) Nanocellulose properties and applications in colloids and interfaces. *Curr. Opin. Colloid Interface Sci.*, **19** (5), 383–396.

26 Ikkala, O., Ras, R.H.A., Houbenov, N., Ruokolainen, J., Pääkkö, M., Laine, J., Leskelä, M., Berglund, L.A., Lindström, T., Ten Brinke, G., and Iatrou, H. (2009) Solid state nanofibers based on self-assemblies: from cleaving from self-assemblies to multilevel hierarchical constructs. *Faraday Discuss.*, **143**, 95–107.

27 Pääkkö, M., Vapaavuori, J., Silvennoinen, R., Kosonen, H., Ankerfors, M., Lindström, T., Berglund, L.A., and Ikkala, O. (2008) Long and entangled native cellulose I nanofibers allow flexible aerogels and hierarchically porous templates for functionalities. *Soft Matter*, **4** (12), 2492.

28 Sehaqui, H., Salajková, M., Zhou, Q., and Berglund, L.A. (2010) Mechanical performance tailoring of tough ultra-high porosity foams prepared from cellulose I nanofiber suspensions. *Soft Matter*, **6** (8), 1824.

29 Huang, J. and Gu, Y. (2011) Self-assembly of various guest substrates in natural cellulose substances to functional nanostructured materials. *Curr. Opin. Colloid Interface Sci.*, **16** (6), 470–481.

30 Teisala, H., Tuominen, M. and Kuusipalo, J. (2014) Superhydrophobic coatings on cellulose-cased materials: fabrication, properties, and applications. *Adv. Mater. Interfaces*, **1** (1) 1300026.

31 Song, J. and Rojas, O.J. (2013) Approaching super-hydrophobicity from cellulosic materials: a review. *Nord. Pulp Pap. Res. J.*, **28** (2), 216–238.

32 Samyn, P. (2013) Wetting and hydrophobic modification of cellulose surfaces for paper applications. *J. Mater. Sci.*, **48** (19), 6455–6498.

33 Young, T. (1805) An essay on the cohesion of fluids. *Philos. Trans. R. Soc. London*, **95**, 65–87.

34 Feng, L., Li, S., Li, Y., Li, H., Zhang, L., Zhai, J., Song, Y., Liu, B., Jiang, L., and Zhu, D. (2002) Super-hydrophobic surfaces: from natural to artificial. *Adv. Mater.*, **14** (24), 1857–1860.

35 Tuteja, A., Choi, W., McKinley, G.H., Cohen, R.E., and Rubner, M.F. (2008) Design parameters for superhydrophobicity and superoleophobicity. *MRS Bull.*, **33** (08), 752–758.

36 Wenzel, R.N. (1936) Resistance of solid surfaces to wetting by water. *Ind. Eng. Chem.*, **28** (8), 988–994.

37 Cassie, A.B.D. and Baxter, S. (1944) Wettability of porous surfaces. *Trans. Faraday Soc.*, **40**, 546–551.

38 Marmur, A. (2003) Wetting on hydrophobic rough surfaces: to be heterogeneous or not to be? *Langmuir*, **19** (20), 8343–8348.

39 Lafuma, A. and Quéré, D. (2003) Superhydrophobic states. *Nat. Mater.*, **2** (7), 457–460.

40 Marmur, A. and Bittoun, E. (2009) When Wenzel and Cassie are right: reconciling local and global considerations. *Langmuir*, **25** (3), 1277–1281.

41 Li, W. and Amirfazli, A. (2005) A thermodynamic approach for determining the contact angle hysteresis for superhydrophobic surfaces. *J. Colloid Interface Sci.*, **292** (1), 195–201.

42 Korhonen, J.T., Huhtamäki, T., Ikkala, O., and Ras, R.H.A. (2013) Reliable measurement of the receding contact angle. *Langmuir*, **29** (12), 3858–3863.

43 Macdougall, G. and Ockrent, C. (1942) Surface energy relations in liquid/solid systems. I. The adhesion of liquids to solids and a new method of determining the surface tension of liquids. *Proc. R. Soc. A*, **180**, 151.

44 Furmidge, C.G. (1962) Studies at phase interfaces. 1. Sliding of liquid drops on solid surfaces and a theory for spray retention. *J. Colloid Sci.*, **17** (4), 309–324.

45 Chow, E.B.D.V. and Robert, T.P. (1983) On the ability of drops or bubbles to stick to non-horizontal surfaces of solids. *J. Fluid Mech.*, **137**, 1–29.

46 Forsberg, P.S., Priest, C., Brinkmann, M., Sedev, R., and Ralston, J. (2010) Contact line pinning on microstructured surfaces for liquids in the Wenzel state. *Langmuir*, **26** (2), 860–865.

47 Pierre, A.C. and Pajonk, G.M. (2002) Chemistry of aerogels and their applications. *Chem. Rev.*, **102** (11), 4243–4266.

48 Shirtcliffe, N.J., McHale, G., Newton, M.I., Perry, C.C., and Pyatt, F.B. (2006) Plastron properties of a superhydrophobic surface. *Appl. Phys. Lett.*, **89** (10), 104106.

49 Jin, H., Tian, X., Ikkala, O., and Ras, R.H.A. (2013) Preservation of superhydrophobic and superoleophobic properties upon wear damage. *ACS Appl. Mater. Interfaces*, **5** (3), 485–488.

50 Jin, H., Nishiyama, Y., Wada, M., and Kuga, S. (2004) Nanofibrillar cellulose aerogels. *Colloids Surf., A*, **240** (1–3), 63–67.

51 Liebner, F., Haimer, E., Wendland, M., Neouze, M.A., Schlufter, K., Miethe, P., Heinze, T., Potthast, A., and Rosenau, T. (2010) Aerogels from unaltered bacterial cellulose: application of $scCO_2$drying for the preparation of shaped, ultra-lightweight cellulosic aerogels. *Macromol. Biosci.*, **10** (4), 349–352.

52 Liebner, F., Haimer, E., Potthast, A., and Rosenau, T. (2012) in *Polysaccharide Building Blocks: A Sustainable Approach to the Development of Renewable Biomaterials* (eds Y. Habibi and L.A. Lucia), John Wiley & Sons, Ltd., pp. 51–103.

53 Olsson, R.T., Samir, M.A., Salazar-Alvarez, G., Belova, L., Ström, V., Berglund, L.A., Ikkala, O., Nogues, J., and Gedde, U.W. (2010) Making flexible magnetic aerogels and stiff magnetic nanopaper using cellulose nanofibrils as templates. *Nat. Nanotechnol.*, **5** (8), 584–588.

54 Jin, H., Kettunen, M., Laiho, A., Pynnönen, H., Paltakari, J., Marmur, A., Ikkala, O., and Ras, R.H.A. (2011) Superhydrophobic and superoleophobic nanocellulose aerogel membranes as bioinspired cargo carriers on water and oil. *Langmuir*, **27** (5), 1930–1934.

55 Aulin, C., Netrval, J., Wågberg, L., and Lindström, T. (2010) Aerogels from nanofibrillated cellulose with tunable oleophobicity. *Soft Matter*, **6** (14), 3298.

56 Korhonen, J.T., Kettunen, M., Ras, R.H.A., and Ikkala, O. (2011) Hydrophobic nanocellulose aerogels as floating, sustainable, reusable, and recyclable oil absorbents. *ACS Appl. Mater. Interfaces*, **3** (6), 1813–1816.

57 Korhonen, J.T., Hiekkataipale, P., Malm, J., Karppinen, M., Ikkala, O., and Ras, R.H.A. (2011) Inorganic hollow nanotube aerogels by atomic layer deposition onto native nanocellulose templates. *ACS Nano*, **5** (3), 1967–1974.

58 Sehaqui, H., Zhou, Q., and Berglund, L.A. (2011) High-porosity aerogels of high specific surface area prepared from nanofibrillated cellulose (NFC). *Compos. Sci. Technol.*, **71** (13), 1593–1599.

59 Kettunen, M., Silvennoinen, R.J., Houbenov, N., Nykänen, A., Ruokolainen, J., Sainio, J., Pore, V., Kemell, M., Ankerfors, M., Lindström, T., Ritala, M., Ras, R.H.A. and Ikkala, O. (2011) Photoswitchable superabsorbency based on nanocellulose aerogels. *Adv. Funct. Mater.*, **21** (3), 510–517.

60 Cervin, N.T., Aulin, C., Larsson, P.T., and Wågberg, L. (2011) Ultra porous nanocellulose aerogels as separation medium for mixtures of oil/water liquids. *Cellulose*, **19** (2), 401–410.

61 Wang, M., Anoshkin, I.V., Nasibulin, A.G., Korhonen, J.T., Seitsonen, J., Pere, J., Kauppinen, E.I., Ras, R.H.A., and Ikkala, O. (2013) Modifying native nanocellulose aerogels with carbon nanotubes for mechanoresponsive conductivity and pressure sensing. *Adv. Mater.*, **25** (17), 2428–2432.

62 Toivonen, M.S., Kaskela, A., Rojas, O.J., Kauppinen, E.I., and Ikkala, O. (2015) Ambient-dried cellulose nanofibril aerogel membranes with high tensile strength and their use for aerosol collection and templates for transparent, flexible devices. *Adv. Funct. Mater.*, **25** (42), 6618–6626.

63 Gavillon, R. and Budtova, T. (2008) Aerocellulose: new highly porous cellulose prepared from cellulose – NaOH aqueous solutions. *Biomacromolecules*, **9** (1), 269–277.

64 Gawryla, M.D., van den Berg, O., Weder, C., and Schiraldi, D.A. (2009) Clay aerogel/cellulose whisker nanocomposites: a nanoscale wattle and daub. *J. Mater. Chem.*, **19** (15), 2118.

65 Wu, Z.Y., Li, C., Liang, H.W., Chen, J.F., and Yu, S.H. (2013) Ultralight, flexible, and fire-resistant carbon nanofiber aerogels from bacterial cellulose. *Angew. Chem. Int. Ed.*, **52** (10), 2925–2929.

66 Puurunen, R.L. (2005) Surface chemistry of atomic layer deposition: a case study for the trimethylaluminum/water process. *J. Appl. Phys.*, **97** (12), 121301.

67 Kettunen, M. (2013) Cellulose nanofibrils as a functional material. Doctoral dissertations. Aalto University, publication series, 114/2013.

68 Jin, H., Marmur, A., Ikkala, O., and Ras, R.H.A. (2012) Vapor-driven marangoni propulsion: continuous, prolonged and tunable motion. *Chem. Sci.*, **3** (8), 2526.

69 Marmur, A. and Ras, R.H.A. (2011) The porous nano-fibers raft: analysis of load-carrying mechanism and capacity. *Soft Matter*, **7** (16), 7382.

70 Sehaqui, H., Zimmermann, T., and Tingaut, P. (2013) Hydrophobic cellulose nanopaper through a mild esterification procedure. *Cellulose*, **21** (1), 367–382.

71 Isogai, A., Saito, T., and Fukuzumi, H. (2011) TEMPO-oxidized cellulose nanofibers. *Nanoscale*, **3** (1), 71–85.

72 Arbatan, T., Zhang, L., Fang, X., and Shen, W. (2012) Cellulose nanofibers as binder for fabrication of superhydrophobic paper. *Chem. Eng. J.*, **210**, 74–79.

73 Geissler, A., Chen, L., Zhang, K., Bonaccurso, E., and Biesalski, M. (2013) Superhydrophobic surfaces fabricated from nano- and microstructured cellulose stearoyl esters. *Chem. Commun.*, **49** (43), 4962.

74 Geissler, A., Biesalski, M., Heinze, T., and Zhang, K. (2013) Formation of nanostructured cellulose stearoyl esters via nanoprecipitation. *J. Mater. Chem. A*, **2** (4), 1107.

75 Geissler, A., Loyal, F., Biesalski, M., and Zhang, K. (2014) Thermo-responsive superhydrophobic paper using nanostructured cellulose stearoyl ester. *Cellulose*, **21** (1), 357–366.

76 Yoon, Y.I., Moon, H.S., Lyoo, W.S., Lee, T.S., and Park, W.H. (2009) Superhydrophobicity of cellulose triacetate fibrous mats produced by electrospinning and plasma treatment. *Carbohydr. Polym.*, **75** (2), 246–250.

77 Thorvaldsson, A., Edvinsson, P., Glantz, A., Rodriguez, K., Walkenström, P., and Gatenholm, P. (2012) Superhydrophobic behaviour of plasma modified electrospun cellulose nanofiber-coated microfibers. *Cellulose*, **19** (5), 1743–1748.

78 Dagnon, K.L., Shanmuganathan, K., Weder, C., and Rowan, S.J. (2012) Water-triggered modulus changes of cellulose nanofiber nanocomposites with hydrophobic polymer matrices. *Macromolecules*, **45** (11), 4707–4715.

79 Anitha, S., Brabu, B., Thiruvadigal, D.J., Gopalakrishnan, C., and Natarajan, T.S. (2013) Optical, bactericidal and water repellent properties of electrospun nano-composite membranes of cellulose acetate and ZnO. *Carbohydr. Polym.*, **97** (2), 856–863.

80 Chen, L., Geissler, A., Bonaccurso, E., and Zhang, K. (2014) Transparent slippery surfaces made with sustainable porous cellulose lauroyl ester films. *ACS Appl. Mater. Interfaces*, **6** (9), 6969–6976.

81 Missoum, K., Belgacem, M., and Bras, J. (2013) Nanofibrillated cellulose surface modification: a review. *Materials*, **6** (5), 1745–1766.

82 Mertaniemi, H., Laukkanen, A., Teirfolk, J.E., Ikkala, O., and Ras, R.H. (2012) Functionalized porous microparticles of nanofibrillated cellulose for biomimetic hierarchically structured superhydrophobic surfaces. *RSC Adv.*, **2** (7), 2882–2886.

83 Bayer, I.S., Steele, A., Martorana, P., Loth, E., Robinson, S.J., and Stevenson, D. (2009) Biolubricant induced phase inversion and superhydrophobicity in rubber-toughened biopolymer/organoclay nanocomposites. *Appl. Phys. Lett.*, **95** (6), 063702.